

RESONANT RELAXATION NEAR A MASSIVE BLACK HOLE:
THE STELLAR DISTRIBUTION AND GRAVITATIONAL WAVE SOURCESCLOVIS HOPMAN¹ AND TAL ALEXANDER^{1,2}

Draft version 11th April 2024

Abstract

Resonant relaxation (RR) of orbital angular momenta occurs near massive black holes (MBHs) where the potential is spherical and stellar orbits are nearly Keplerian and so do not precess significantly. The resulting *coherent* torques efficiently change the magnitude of the angular momenta and rotate the orbital inclination in all directions. As a result, many of the tightly bound stars very near the MBH are rapidly destroyed by falling into the MBH on low-angular momentum orbits, while the orbits of the remaining stars are efficiently randomized. We solve numerically the Fokker-Planck equation in energy for the steady state distribution of a single mass population with a RR sink term. We find that the steady state current of stars, which sustains the accelerated drainage close to the MBH, can be ~ 10 larger than that due to *non-coherent* 2-body relaxation alone. RR mostly affects tightly bound stars, and so it increases only moderately the total tidal disruption rate, which is dominated by stars originating from less bound orbits farther away. We show that the event rate of gravitational wave (GW) emission from inspiraling stars, originating much closer to the MBH, is dominated by RR dynamics. The GW event rate depends on the uncertain efficiency of RR. The efficiency indicated by the few available simulations implies rates ~ 10 times higher than those predicted by 2-body relaxation, which would improve the prospects of detecting such events by future GW detectors, such as *LISA*. However, a higher, but still plausible RR efficiency can lead to the drainage of all tightly bound stars and strong suppression of GW events from inspiraling stars. We apply our results to the Galactic MBH, and show that the observed dynamical properties of stars there are consistent with RR.

Subject headings: black hole physics — Galaxy: center — stellar dynamics — gravitational waves

1. INTRODUCTION

Galactic nuclei with massive black holes (MBHs) are stellar systems with relaxation times that are often shorter than the age of the Universe. In that case the distribution function (DF) of the system may approach a steady state. This steady state is determined by the boundary conditions (an inner sink, such as the tidal radius of the MBH, and an outer source at the interface with the host galaxy) and by the mutual interactions between the stars themselves. The nature of the “microscopic” interactions between the stars determines the rate at which the system relaxes to its steady state.

With the notable exception of N -body simulations (e.g. Baumgardt, Makino & Ebisuzaki 2004a, 2004b; Preto, Merritt & Spurzem 2004; Merritt & Szell 2005), analyses of the evolution of the DF near a MBH have almost exclusively relied on the assumption that the mechanism through which stars exchange angular momentum and energy is dominated by *uncorrelated two-body interactions* (Chandrasekhar 1943; see Binney & Tremaine 1987 for a more recent discussion). This assumption is made in Fokker-Planck models (e.g. Bahcall & Wolf 1976 [hereafter BW76]; Bahcall & Wolf 1977 [hereafter BW77]; Cohn & Kulsrud 1978; Murphy, Cohn & Durisen 1991), where the microscopic interactions are expressed by the diffusion coefficients, and in Monte Carlo simulations (e.g. Shapiro & Marchant 1979; Marchant & Shapiro 1979, 1980; Freitag & Benz 2001, 2002). Stars around MBHs are described as moving in the smooth aver-

age potential of the MBH and the stars, and the scattering by the fluctuating part of the potential is modeled as a hyperbolic Keplerian interaction between a passing star and a test star. The scattering effects accumulate non-coherently in a random-walk fashion.

The (non-resonant) relaxation time T_{NR} can be defined as the time T_E it takes for the negative specific energy E ($\sqrt{v^2/2}$ of a typical star (hereafter “energy”) to change by order unity. This is also the time T_J it takes for its specific angular momentum J (hereafter “angular momentum”) to change by an amount of order $J_c(E)$, the maximal (circular orbit) angular momentum for that energy³. In a spherical potential $J_c = G M_\bullet + N(>E)M_\star \sqrt{2E}$, where M_\bullet is the MBH mass, M_\star is the stellar mass and $N(>E)$ is the number of stars with orbital energies above E (more bound than E). On Keplerian orbits $J_c = \sqrt{GM_\bullet a}$, where a is the semi-major axis. When relaxation is dominated by uncorrelated two-body interactions, the “non-resonant” relaxation time T_{NR} of stars of mass M_\star can be written in the Keplerian regime as

$$T_{NR} = A \frac{M_\bullet^2}{M_\star} \frac{P(a)}{N(<a)} \quad (M_\bullet, M_\star); \quad (1)$$

where $P = 2\pi \sqrt{a^3/(GM_\bullet)}$ is the orbital period and A is a dimensionless constant which includes the Coulomb logarithm. We assume throughout a single mass stellar population; for numerical estimates we assume $M_\star = 1 M_\odot$.

The assumption of uncorrelated two-body interactions is well-justified in many systems, such as globular clusters.

³ Throughout this paper, “angular momentum relaxation time” means the time it takes until J is changed by order J_c , rather than by order J . The time-scale for changes by order $J < J_c$ is shorter than the angular momentum relaxation time by a factor $(J=J_c)^2$.

¹ Faculty of Physics, Weizmann Institute of Science, POB 26, Rehovot 76100, Israel; clovis.hopman@weizmann.ac.il, tal.alexander@weizmann.ac.il

² Incumbent of the William Z. & Eda Bess Novick career development chair
Electronic address: clovis.hopman, tal.alexander@weizmann.ac.il

However, Rauch & Tremaine (1996, hereafter RT96) showed that this does not hold for motion in potentials with certain symmetries, in particular for Keplerian motion in the potential of a point mass where the orbits do not precess because of the 1 : 1 resonance between the radial and azimuthal frequencies. This is to a good approximation the case for stars orbiting close, but not too close to a MBH, since wider orbits precess due to the potential of the enclosed stellar mass, while tighter orbits precess due to General Relativity (GR). As long as the precession timescale t_p (the time to change the argument of the periastron by π) is much longer than the orbital period, the orbits effectively remain fixed in space over times $P \ll t_p$ and the interactions are correlated. The orbiting stars can then be represented by one-dimensional elliptical “wires” whose mass density varies along the wire in proportion to the time spent there (RT96). In this picture the interaction between two stars can be described as the torque between two wires. This results in mutual changes in *both* the direction and the magnitude of the angular momenta. Following RT96, we denote such RR, which also changes the magnitude of \mathbf{J} , *scalar RR*. The change grows coherently ($\propto t$) on timescales $t \ll t_p$ and non-coherently ($\propto t^{1/2}$) on longer timescales $t \gg t_p$, where T_{RR} is the “resonant relaxation” (RR) timescale for the angular momentum (Eq. 3). Generally, $T_{RR} \propto T_{NR}$ when $M \gg N \langle a \rangle M$ (see Eq. 5). Since the potential of the wires is stationary on time-scales $\ll t_p$, they do not exchange energy, and the energy relaxation timescale remains long, $T_E \gg T_{NR}$, even in the resonant regime. The mechanism of RR is reminiscent of the Kozai mechanism in triple stars (Kozai 1962).

A more restricted type of RR occurs in any spherical potential, where the vector \mathbf{J} is conserved, but \mathbf{J} precesses. In that case the orbital rosette can be represented by a mass disk extending between the orbital periastron and apo-apse. The mutual torques exerted by such azimuthally symmetric disks change *only* the direction of \mathbf{J} , but not its magnitude. This type of RR persists even in the presence of GR precession. Following RT96, we denote such RR, which changes only the direction of \mathbf{J} , *vector RR*. The significance of the distinction between scalar and vector RR is that scalar RR can deflect stars into “loss-cone” orbits ($\mathbf{J} \cdot \mathbf{J}_c \leq \mathbf{J} \cdot \mathbf{0}$) where they fall into the MBH, either directly (“infall”) or gradually (“inspiral”), whereas vector RR can only randomize the orbital orientation, but cannot affect the loss rate.

In this paper we explore the consequences of RR on the stellar DF and on the infall and inspiral rates. The mechanism of RR is briefly reviewed in §2. The Galactic Center (GC) model is defined and the assumptions and approximations are discussed in §3. In §4 we solve the Fokker-Planck equation in energy and analyze the effects of RR on the DF (§4.2) and on the stellar current (§4.3). In §5 we discuss the observational consequences of RR, such as the event rates of tidal disruption (§5.1.1) and gravitational wave (GW) emission (§5.1.2). We discuss our results in the context of the young, non-relaxed stars in the GC (§5.2). We discuss and summarize our results in §6.

2. RESONANT RELAXATION

The resonant relaxation time T_{RR} is estimated by evaluating $\mathbf{J} \cdot \mathbf{J}_1$, the coherent change in the magnitude of the specific angular momentum up to a time t_1 . The change $\mathbf{J} \cdot \mathbf{J}_1$ is then the step size (“mean free path”) for the non-coherent growth of the angular momentum over times $t > t_1$. Two nearby stars with semi-major axes a exert a mutual specific torque

$G M \propto a$. Within a distance a from the MBH the net torque on a test star fluctuates away from zero as $\sqrt{N \langle a \rangle} G M \propto a$ and

$$\mathbf{J} \cdot \mathbf{J}_1 = \sqrt{N \langle a \rangle} G M \propto a t_1 \quad (2)$$

For $t > t_1$ the torques on a particular star-wire become random, and the change in angular momentum grows in a random walk fashion with a timescale $T_{RR} \propto (\mathbf{J} \cdot \mathbf{J}_1)^{-2} t_1$, defined here as

$$T_{RR} = A_{RR} \frac{N \langle E \rangle P^2(E)}{2 \langle E \rangle t_1}, \quad \frac{A_{RR}}{N \langle a \rangle} \frac{M}{M \propto} \frac{P^2(a)}{t_1}; \quad (3)$$

where $N M \propto (M + N M \propto)$, A_{RR} is a numerical factor of order unity, to be determined by simulations, and the last approximate equality holds in the Keplerian regime. The N -body simulations of RT96 indicate that $A_{RR}^S = 3.56$ for scalar RR (§2.1) and $A_{RR}^V = 0.31$ for vector RR (§2.2) (see their Eqs. 8, 15 and table 4 for s and v ; $A_{RR}^{S/V} \propto \frac{2}{s^{3/2}}$). We adopt these values here. We verified these result, to within an order of unity, by carrying a few full small scale N -body simulations. Our simulations exhibited a substantial scatter in the value of A_{RR} , as already noted by RT96. This introduces an uncertainty in quantitative estimates of the efficiency of RR. Further detailed analysis and simulations, outside the scope of this study, are needed to refine these numerical estimates.

2.1. Scalar resonant relaxation

Over most of the relevant phase space, the precession is due to the deviations from pure Keplerian motion caused by the potential of the extended stellar cluster (“mass precession”). This occurs on a timescale $t_p = t_M$, which assuming $N \langle a \rangle M \propto M$ and after averaging on \mathbf{J} , can be expressed as

$$t_M = A_M \frac{M}{N \langle a \rangle M \propto} P(a); \quad (4)$$

and where A_M is a dimensionless constant. For simplicity we adopt here $A_M = 1$, the value for circular orbits. The \mathbf{J} -averaged RR timescale can then be written as

$$T_{RR}^M = A_{RR} \frac{M}{M \propto} P(a) = \frac{A_{RR}}{A} \frac{M \propto}{M} N \langle a \rangle T_{NR}; \quad (5)$$

Since $T_{RR}^M \propto T_{NR}$ for small a where $N \langle a \rangle M \propto M$, the RR rate of angular momentum relaxation is much higher than the rate of energy relaxation in the resonant regime. This qualitative analysis has been verified by detailed numerical N -body simulations by RT96 and by Rauch & Ingalls (1998, hereafter RI98).

For most of \mathbf{J} -space, orbital precession is dominated by the mass of the stellar cluster and the RR relaxation timescale is well approximated by $T_{RR} \propto T_{RR}^M$, which is a function of energy only. However, when the orbital periastron is very close to the MBH, precession is dominated by GR effects (“GR precession”). This is important for our analysis of the inspiral rate of GW sources (§5.1.2). In this case the timescale for precession is given by $t_p = t_{GR}$, which is a strong function of \mathbf{J} ,

$$t_{GR} = \frac{8}{3} \frac{J}{J_{LSO}}^2 P; \quad (6)$$

where

$$J_{\text{LSO}} = \frac{4GM}{c} \quad (7)$$

is the angular momentum of the last stable orbit (LSO) for an orbit of specific kinetic energy c^2 . Generally, both precession mechanisms operate, and the scalar RR timescale $T_{\text{RR}}^s(E; J)$ is given by substituting $1=t_1 = J_1=t_M = 1=t_{\text{GR}} J$ in Eq. (3), where the opposite signs reflect the fact that mass precession is retrograde whereas GR precession is prograde. Thus, the scalar RR timescale is

$$T_{\text{RR}}^s = \frac{A_{\text{RR}}}{N(<a)} \frac{M}{M_\odot} P^2(a) \frac{1}{t_M} \frac{1}{t_{\text{GR}}} ; \quad (8)$$

When $t_{\text{GR}} = t_M$ and GR precession dominates, the RR timescale is (Eq. 5)

$$T_{\text{RR}}^{\text{GR}} = \frac{3}{8} A_{\text{RR}} \frac{M}{M_\odot} \frac{J_{\text{LSO}}^2}{J} \frac{P(a)}{N(<a)} ; \quad (9)$$

The fact that scalar RR becomes much less efficient due to GR precession is crucial for the viability of GW emission from inspiraling stellar objects (“extreme mass-ratio inspiral sources”, EMRIs), since it allows compact remnants to be very rapidly deflected to strongly relativistic orbits, but then stall “on the brink” and instead of falling directly into the MBH, inspiral into it gradually by the emission of GW. We return to this issue in §5.1.2.

We analyze below the dynamics of scalar RR and its effects on the stellar DF, both numerically (§4) and by Monte-Carlo simulations (§5). These two approaches require different formulations of the RR timescale. The numerical analysis is carried out in the 1D E -space, where the J -dependences are absorbed in the J -averaged terms. For this purpose we use the relation $d(J^2)=J_c^2 = dt T_{\text{RR}}^s(E; J)$ (Eqs. 8) to define the J -averaged time it takes a star to random-walk from $J = J_c(E)$ to the loss-cone $J = J_{\text{lc}}$ as

$$T_{\text{RR}}^s(E) = \frac{1}{J_c^2} \int_{J_{\text{lc}}}^{J_c} dJ^2 T_{\text{RR}}^s(E; J) ; \quad (10)$$

Since at low energies T_{RR}^s / P , it initially decreases with E toward the MBH. However, at very large energies near the MBH, where GR precession becomes important ($J_{\text{LSO}}=J_c(E) \rightarrow 1$), T_{RR}^s increases again (Fig. 7). The Monte Carlo simulations are carried out in 2D (E, J) -space. For this purpose we define a general expression for the scalar angular momentum relaxation time, T_J^s , which applies in any regime (Eqs. 1, 3, 8; see also footnote 3).

$$T_J^s(E; J) = \frac{1}{T_{\text{NR}}(E)} + \frac{1}{T_{\text{RR}}^s(E; J)} ; \quad (11)$$

2.2. Vector resonant relaxation

Vector RR grows coherently ($\propto t$) on timescales $t = t$, where t is the timescale for a change of order unity in the total gravitational potential Φ caused by the changes in the stellar potential Φ_\star due to the realignment of the stars as they rotate by θ on their orbits,

$$t = \frac{\Phi}{\dot{\Phi}} = A_\star \frac{N^{1/2} P}{2} \frac{1}{2} A_\star \frac{M}{M_\odot} \frac{P}{N^{1/2}} ; \quad (12)$$

where A_\star is a dimensionless constant of order unity, and where the last approximate equality holds for $N M_\odot \gg M$. For simplicity we adopt here $A_\star = 1$. In analogy to scalar RR (Eq. 2), the maximal coherent change in J is

$$J - J_0 = J - J_0 = J_0 ; \quad (13)$$

that is, J rotates by an angle $\mathcal{O}(1)$ already during the coherent phase. On timescales $t = t$, $J - J_0$ cannot grow larger, as it already reached its maximal possible value, but the orbital inclination angle is continuously randomized non-coherently ($\propto t^{1/2}$) on the vector RR timescale (Eq. 3),

$$T_{\text{RR}}^v = 2A_{\text{RR}}^v \frac{N^{1/2} P(E)}{(E)} P(E) \frac{2A_{\text{RR}}^v}{M_\odot} \frac{P(a)}{N^{1/2}(<a)} ; \quad (14)$$

where the last approximate equality holds for $N M_\odot \gg M$.

Note that while the torques driving scalar and vector RR are the same, vector RR is much more efficient than scalar RR, $T_{\text{RR}}^v \ll T_{\text{RR}}^s$, due to the much longer coherence time $t = N^{1/2} t_M = t_M$. Furthermore, vector RR proceeds irrespective of any precession mechanisms that limit the efficiency of scalar RR.

3. A STELLAR CLUSTER WITH A MASSIVE BLACK HOLE: MODEL AND ASSUMPTIONS

In this section we state our assumptions, approximations and definitions, many of which are commonly used in the analysis of stellar systems with MBHs. Since the GC is the best studied case of a stellar cluster with a MBH, and since it is representative of typical *LISA* targets, we scale the parameters to values appropriate for this system. Our goal is to find the stellar DF in presence of RR. A full solution in (E, J) -space is complex and is not attempted here. For simplicity, the analysis carried out here is in E -space only and it assumes an underlying spherical symmetry. The J -dependent loss-cone terms are approximated by their J -averaged effective terms, which are functions of E only.

3.1. Distribution in energy space

Recent observations show that a tight empirical relation exists between the mass of MBHs, M_\bullet , and the velocity dispersion σ of their host bulge or galaxy (Ferrarese & Merritt 2000; Gebhardt et al. 2000),

$$M_\bullet = 1.3 \times 10^6 M_\odot \left(\frac{\sigma}{200 \text{ km s}^{-1}} \right)^4 ; \quad (15)$$

where σ is measured at the galaxy’s effective radius (Tremaine et al. 2002). Both the exponent and the prefactor have small uncertainties, which we ignore here. The Galaxy obeys the M_\bullet - σ relation, with $M_\bullet = 3 \times 10^6 M_\odot$, and 75 km s^{-1} (Tremaine et al. 2002).

The MBH dominates the dynamics of stars within its “Bondi radius”, or radius of influence,

$$r_h = \frac{GM_\bullet}{2\sigma^2} = 2 \text{ pc} \left(\frac{M_\bullet}{3 \times 10^6 M_\odot} \right) \left(\frac{75 \text{ km s}^{-1}}{\sigma} \right)^2 \quad (16)$$

$$= 2 \text{ pc} \left(\frac{M_\bullet}{3 \times 10^6 M_\odot} \right)^{1/2} ; \quad (17)$$

where in the last step we used the M_\bullet - σ relation. Within r_h the system is approximately Keplerian, and deviations from

Keplerian motion become important only for times $t \gg P$, where $P(E) = 2\pi \frac{a^3}{GM} \sqrt{2E}$ is the orbital period and the energy is $E = GM/a = r/v^2$.

We assume a single mass population with an underlying spherically symmetric DF, so that $f(\mathbf{x};\mathbf{v}) = f(E)$ (stars per phase space volume $d^3x d^3v$). Following BW76 we assume that for $r > r_h$ the DF is Maxwellian,

$$f(E) = \frac{n_h}{(2\pi)^{3/2} v_h^3} e^{-E/v_h^2} \quad (r > r_h); \quad (18)$$

where $n_h \approx 4 \times 10^6 \text{ pc}^{-3}$ is the number density at r_h in the GC assuming a mean mass of $1 M_\odot$ (Genzel et al. 2003) and where $v_h = 75 \text{ km s}^{-1}$ is the 1D velocity dispersion at r_h . For Keplerian orbits, the density $n(E)$ (stars per dE) is

$$n(E) = \frac{P}{2} \frac{1}{(GM)^{3/2}} E^{5/2} f(E); \quad (19)$$

the density $n(r)$ (stars per d^3x) is

$$n(r) = 4\pi \int_0^\infty \frac{1}{2} \frac{GM}{r^3} dE f(E) \frac{GM}{r} E; \quad (20)$$

and the density $n(a)$ (stars per da) is

$$n(a) = 4\pi \int_0^\infty \frac{1}{2} (GM)^{3/2} a^{1/2} f \frac{GM}{2a} : \quad (21)$$

Two stellar components contribute to the local stellar density at radius r . One is the tightly bound stars with energy $E \ll GM/r$, or $a \gg r$. The other is the unbound, or marginally bound stars with energy $E \approx GM/r$ (or $a \approx r$) and high eccentricities, which spend only a small fraction of their orbit inside r . When unbound stars dominate the local population, for example because RR or stellar collisions have destroyed most of the tightly bound stars there, the density profile is given by

$$n_u(r) = 4\pi \int_0^\infty \frac{1}{2} dE f(E) \frac{GM}{r} E / r^{1/2} : \quad (22)$$

We express the local relaxation time, which generally depends on the nature of the relaxation process and on radius, in terms of a reference time T_h , which we define as the NR relaxation time at r_h ,

$$T_h = \frac{3}{16} \frac{r}{n_h} \frac{1}{(GM)^{3/2} \ln} \frac{M}{10^6 M_\odot} \quad (23)$$

where the last equality assumed the $M - r$ relation and the stellar density in the GC. The Coulomb factor is $\ln \frac{r_{\text{max}}}{r_{\text{min}}} = \ln \frac{M}{M_\odot}$ (BW76), where $r_{\text{max}} = r$ is the maximal impact parameter for perturbations by stars interior to r , and r_{min} is the minimal impact parameter for small deflections, $r_{\text{min}} = GM/v^2 = (M/M_\odot) r$. The local NR relaxation time may be quite different from T_h when the density distribution of the system strongly deviates from the steady state configuration $n(r) \propto r^{-4}$ (§4.2).

3.2. The loss-cone

At high enough energy the DF vanishes, $f(E > E_D) = 0$, because stellar objects cannot survive close to the MBH. The value of E_D depends on the process that destroys the stars. If they are compact objects, they fall directly into the MBH or inspiral into it by GW emission. If they are main sequence stars, they are destroyed by disruptive stellar collisions in the high density cusp around the MBH, or are tidally captured and heated until disruption, or are tidally disrupted when their orbital periapse r_p falls below the tidal disruption radius, $r_t = (M/M_\odot)^{1/3} R_\odot$.

Stars are destroyed by the MBH either by scattering or decaying in E-space to the point where $E > E_D$, or by scattering in J-space to the point where $J < J_{\text{lc}} = \frac{2GM}{r_t}$ (or $r_p < r_t$). Scattering in J-space is by far more efficient (Frank & Rees 1976; Lightman and Shapiro 1977; see footnote 3), and the tidal disruption rate is dominated by stars on low-E and low-J orbits. Stars enter the loss-cone, defined by $J < J_{\text{lc}}$, in two regimes of phase-space, depending on their orbital energy, which determines the ratio between the angular momentum change per orbit, $\Delta J(E)$, and J_{lc} . For small energies (long periods), $J \ll J_{\text{lc}}$. In this “full loss-cone” (or “kick”) regime, the DF remains essentially unmodified by the existence of a loss-cone. For high energies (short periods) near the MBH, $J \approx J_{\text{lc}}$. In this “empty loss-cone” (or “diffusive”) regime stars slowly diffuse into the loss-cone and are then promptly destroyed on a dynamical time, and the DF is modified by the existence of the loss-cone. The stellar density vanishes inside the loss-cone, $n(E; J < J_{\text{lc}}) = 0$, and gradually falls to zero toward it, $n(J) \propto J \ln(J/J_{\text{lc}})$ for $J \approx J_{\text{lc}}$ (Lightman & Shapiro 1977). This also modifies somewhat the DF in E-space. Note that scalar RR is typically efficient only deep in the empty loss-cone regime, where mass precession is negligible.

There is a critical energy where $J(E) = J_{\text{lc}}$, that demarcates the transition between the empty and full loss-cone regimes. The size of the loss-cone, and therefore the critical energy, depends on the nature of the loss-process. The critical energy for prompt stellar disruption E_p , corresponds to a distance scale of r_h where $E = E_h$ (Eq. 16). Most of the contribution to the stellar destruction rate is from stars with $E \approx E_p$. Similarly, there is a critical energy for stellar destruction by GW inspiral, E_{GW} . GW inspiral takes much longer than direct disruption. Unless the star starts out on a short-period (high-E) orbit, it will be scattered again directly into the MBH, or to a high-J orbit where GW dissipation is negligible. Thus, $E_{\text{GW}} \approx E_p$ (Alexander & Hopman 2003).

We adopt below for numerical calculations the values of the critical energies in the GC, where for consistency with our assumed single mass population, we consider only prompt disruption and GW inspiral at the last stable orbit, $J_{\text{lc}} = 4GM/c$. In the GC, the semi-major axes corresponding to these critical energies are $a_p = 0.27 \text{ pc}$ and $a_{\text{GW}} = 0.02 \text{ pc}$ (see Fig. 6). Thus, our model describes a population of compact objects, and our predicted prompt disruption rates will be slightly lower than the actual tidal disruption rates, which occur at the somewhat larger $J_{\text{lc}} = \frac{2GM}{r_t}$ and thus have a lower critical energy, closer to E_h .

A complete treatment of the loss-cone problem involves the solution of the Fokker-Planck equation in $(E; J)$ -space (Cohn & Kulsrud 1978). However, an approximate solution can be obtained by solving the Fokker-Planck equation in E-space only, while accounting for the loss-cone by adding sink terms

to the equation (BW77). This is the approach we adopt here. The tidal disruption rate due to NR relaxation has been discussed extensively in the literature (see e.g. Lightman and Shapiro 1977; Frank & Rees 1976; Cohn & Kulsrud 1978; Syer & Ulmer 1999; Magorrian & Tremaine 1999; Alexander & Hopman 2003; Merritt & Poon 2004; Wang & Merritt 2004; Hopman & Alexander 2005; Baumgardt et al. 2005). The differential NR loss-cone diffusion rate (stars per $dE dt$) is estimated to be of the order

$$\dot{n}_{NR}(E) = n(E) T_{NR}(E); \quad (24)$$

neglecting here the weak logarithmic J -dependence that expresses the depletion of phase space near the loss-cone. When RR is the dominant relaxation process, then for timescales t_{\perp} the differential loss-cone refilling rate is⁴

$$\dot{n}_{RR}(E) = n(E) T_{RR}^S(E); \quad (25)$$

Note that vector RR does not enter into the Fokker Planck equation and does not play a role in the diffusion in E -space since the system is assumed to be spherically symmetric, and vector RR does not change J .

4. DENSITY PROFILE NEAR A MASSIVE BLACK HOLE

4.1. Fokker-Planck energy equation with resonant relaxation

Following BW76, we define the dimensionless quantities

$$g = (2 \frac{2}{h})^{3=2} n_h^{-1} f; \quad x = E = \frac{2}{h}; \quad \tau = t T_h; \quad (26)$$

and write the Fokker-Planck equation⁵ as

$$\frac{\partial g(x; \tau)}{\partial \tau} = x^{5=2} \frac{\partial Q(x; \tau)}{\partial x} - R_{NR}(x; \tau) - R_{RR}(x; \tau); \quad (27)$$

where the current $Q(x)$, defined to be the net rate at which stars flow to energies $> x$, is given by (BW76)

$$Q(x; \tau) = \int_1^{x_D} dy g(x; \tau) \frac{\partial g(y; \tau)}{\partial y} - g(y; \tau) \frac{\partial g(x; \tau)}{\partial x} \quad \text{for } x(x; y) g^{3=2}; \quad (28)$$

The sink terms R_{NR} and R_{RR} represent the J -averaged differential loss rate of stars per energy interval, by NR and RR respectively, due the existence of a loss-cone in J -space. This is an approximate substitute for the full $2+1$ treatment.

The NR sink term $R_{NR}(x; \tau)$ is expressed by the form (Eq. B1 in appendix B) proposed by BW77, which smoothly interpolates between the empty and the full loss-cone regimes and approximates the logarithmic depletion of phase space near the loss-cone boundary (§3.2). In the empty loss-cone regime, which is of interest here,

$$R_{NR}(x; \tau) / g(x; \tau) \approx \log(x_D = 4x); \quad (29)$$

⁴ Eq. (25) differs from the corresponding term in RT96, which applies only for timescales t_{\perp} , and an isotropic DF. The rate predicted by Eq. (25) is in good agreement with the values obtained by the N -body simulations of RI98.

⁵ Equation (27) is written in the form of a particle conservation relation, which, as shown by BW76, is equivalent to the usual Fokker-Planck form $\partial f / \partial t = -D_x \partial f / \partial x + D_{xx} \partial^2 f / \partial x^2$, where D_x and D_{xx} are the diffusion coefficients.

This quadratic behavior arises since a fraction $g(x; \tau)$ of the stars is accreted per local relaxation time, which is itself proportional to $1/g(x; \tau)$.

The RR sink term R_{RR} is expressed by (Eqs. 5, 25)

$$R_{RR}(x; \tau) = g(x; \tau) / T_{RR}(x); \quad (30)$$

where $T_{RR}(x) = T_{RR}^S(E) = T_h$ is the dimensionless J -averaged RR time, defined in Eq. (10).

The RR efficiency factor in Eq. (27) parametrizes the uncertainties in the efficiency of RR and in the approximations involved in Eq. (30), for example the effect of the partial depletion of phase-space outside the loss-cone (note that the depletion is small, see RI98 fig. [2a]). For simplicity, we assume that η is a constant. We expect $\eta \ll 1$, and show below that the choice $\eta = 1$ yields results that are consistent with those of RT96 and RI98, but we also explore RR for a range of η values to determine the robustness of our results. The RR sink term becomes negligible compared to the NR sink term for lower energies, where $T_{RR} > T_h$ (Fig. 7).

We follow BW76 by assuming as boundary conditions

$$g(x < 0; \tau) = e^x; \quad g(x = x_D; \tau) = 0; \quad (31)$$

The first boundary condition for $x < 0$ expresses the assumption of a thermal reservoir at the radius where the stars are no longer bound to the MBH (Eq. 18). In reality, they are bound to the total enclosed mass of the MBH and stars, however the BW76 treatment neglects the stellar mass and assumes Keplerian motion around the MBH. The second expresses the existence of a mass-sink at energy x_D . Because of the large dynamical range in the problem, it is more convenient for numerical purposes to express Eqs. (27-31) in logarithmic energy (see appendix A).

4.2. The effects of RR on the stellar distribution function

Here we explore the effect of RR on the steady state DF. We begin by checking the numerical convergence of Eq. (27) to the BW76 solution, $f(E) / E^p$ with $p = 1=4$ for $E_h \leq E \leq E_D$, which is obtained under the assumption that the E -dependent J -averaged sink terms can be neglected, $R_{NR} = R_{RR} = 0$, and that the disruption of stars by the MBH can be expressed by the boundary condition $f(E > E_D) = 0$. Figure (1) confirms that the DF indeed converges to this solution on a relaxation timescale, and we also verified that this holds irrespective of the initial DF assumed. Rapid conversion was also confirmed by the N -body simulations of Merritt & Szell (2005). The BW76 DF corresponds to a power-law density profile $n(r) / r^{-p}$ with $p = 3=2 = 7=4$ (equation 20). Since $T_{NR}(E) / P(E) = N(>E)$, and $T_{NR}(E = \frac{2}{h}) = T_h$, the implied *local* NR time is

$$T_{NR}(E) = T_h E = \frac{2}{h}^{3=2}; \quad (32)$$

We now add back the NR and RR sink terms and solve the full problem. Figure (2) shows the results of the steady state solution of equation (27) for several values of η . The $\eta = 0$ case (NR only) reproduces the solution studied by BW77, who showed that the presence of the NR sink term does not change the power-law behavior and index of the DF. We find, as expected, that for low energies where RR is negligible, neither does the presence of the RR sink term. At higher energies, the response of the DF depends on the efficiency of RR. For $\eta \approx 10$, RR is so efficient that it exponentially depletes

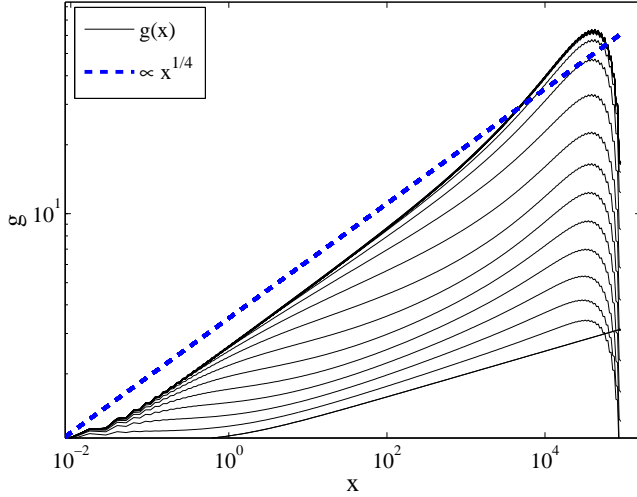


FIG. 1.— The evolution of the stellar DF to a steady-state $E^{1/4}$ cusp (BW76) by E-diffusion only (no loss-cone effects: $R_{NR} = R_{RR} = 0$). The dimensionless sink energy is at $x_D = 10^5$, approximately appropriate for the tidal radius in the GC. Lines show $g(x; t)$ at intervals of $t = 0.07$, with the lowest curve indicating the initial DF (arbitrarily assumed here to be $g(x; 0) \propto x^{0.1}$). The system was integrated up to $2T_h$; the steady state DF is reached after $0.8T_h$. For comparison, an $x^{1/4}$ power-law is also shown.

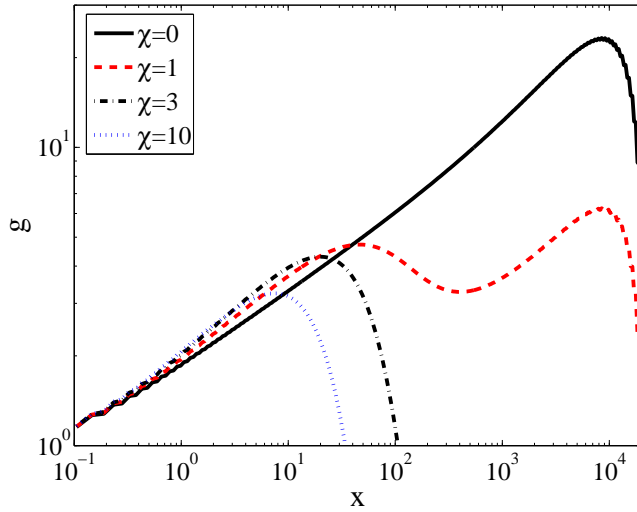


FIG. 2.— Growth of a cusp in presence of RR, with the same initial conditions as in Fig. (1) in the presence of the NR and RR sink terms for RR efficiency factors of $\chi = 0; 1; 3; 10$. For RR efficiency factor $\chi = 3$, RR leads to an exponential cutoff of the DF at high energies.

the high energy end of the DF. However, for the likely efficiency factor $\chi = 1$, GR precession at high energies limits the efficiency of RR (cf Fig. 7), and the DF is not completely depleted, but continues to rise toward $E \rightarrow E_D$ after a moderate initial drop.

4.3. The effects of RR on the stellar current

The solution of the Fokker-Planck equation determines the stellar current $Q(x)$ into the MBH. This in turn determines the rates and modes of stellar capture by the MBH. Since most of the contribution to prompt infall events comes from orbits with energy $x \sim x_p$, and to GW inspiral from $x \sim x_{GW}$ (§3.2, §5), the current at these critical energies determines the prompt infall and gravitational inspiral event rates. In the GC, $x_p = 2.7$ and $x_{GW} = 58$ (§3.2).

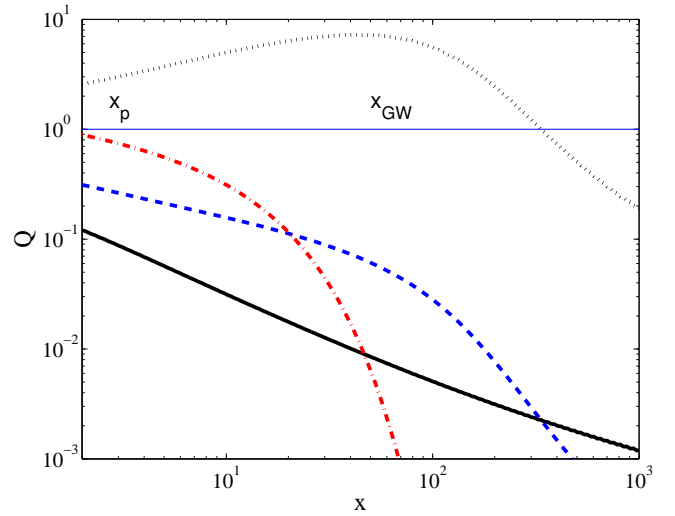


FIG. 3.— The steady state current Q as function of dimensionless energy x , for various choices of the RR efficiency parameter χ . Solid line: $\chi = 0$ (NR only). Dashed line: $\chi = 1$. Dot-dashed line: $\chi = 10$. The capture rates are determined by the value of the current at the critical energies (shown here at values typical for the GC, §5.1.1, §5.1.2). The dotted line is the ratio Q_1/Q_0 between the currents of the $\chi = 1$ and $\chi = 0$ cases. At x_{GW} , $Q_1/Q_0 \approx 8$, so the GW inspiral rate is dominated by RR. At x_p , $Q_1/Q_0 \approx 3$ so prompt infalls are somewhat enhanced by RR, as found by RT96 and R198. When $\chi = 10$, RR is so efficient that it evacuates a large fraction of the stars at energies higher than x_{GW} , and the GW inspiral rate is suppressed relative to the $\chi = 1$, whereas the prompt infall rate is further enhanced.

The rate at which stars flow toward the MBH is given by

$$\dot{I}(E; t) = I_0 Q(x; t); \quad (33)$$

where the dimensional current scale is set by

$$I_0 = \frac{8}{3} \frac{\sigma^2}{2} r_h^3 n_h \frac{(GM_\bullet)^2 \ln n_h}{h^3} \approx \frac{N_h}{T_h}; \quad (34)$$

For non-equilibrium DFs, $Q \neq 1$, and there is a large current $I \gg I_0$. The “sink-less” BW76 solution (§4.2) has a steady state “zero-current” ($0 < Q \leq 1$) solution that is E-independent and is strongly suppressed by the bottle-neck at E_D . The presence of the loss-cone, as expressed by the NR and RR sink terms, modifies the DF at high energies and shifts the effective high-energy boundary to lower energies. As a result, Q increases well above the zero-current solution and becomes E-dependent.

Figure (3) shows the current $Q(x)$ for several values of the RR efficiency factor χ . The accelerated relaxation due to RR increases the current above the values induced by NR only. For $\chi = 1$ the largest enhancement is attained at about the critical energy for GW. When $\chi \approx 10$, RR is so efficient that the current depletes the DF already at energies $x \sim x_{GW}$. As a consequence, the current drops to zero at $x > x_{GW}$, and therefore so does the GW inspiral event rate (which is $\propto Q(x_{GW})$, see eq. [37]). Figure (4) shows separately the contributions of the NR and RR sink terms in Eq. (27) to the total capture rate, and demonstrates that far from the MBH (low-E), where most tidally disrupted stars originate, NR dominates the capture rate, whereas at closer distances (high-E), where GW inspiral stars originate, RR dominates the capture rate (see also Fig. 7 below).

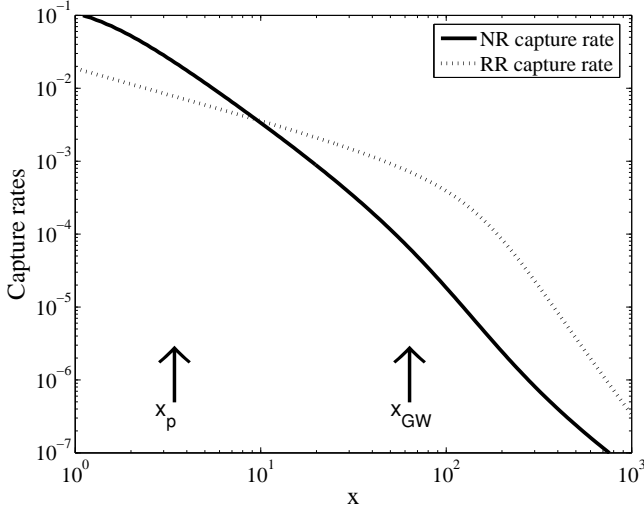


FIG. 4.— The differential capture rates $x^{5/2}R_{NR}$ (solid line) and $x^{5/2}R_{RR}$ with $\eta = 1$ (dashed line) as function of dimensionless energy x . At high energies near x_{GW} , where GW sources originate, captures are dominated by RR. Prompt infall is dominated by NR in the region near x_p , in the transition between the full and empty loss-cone regimes.

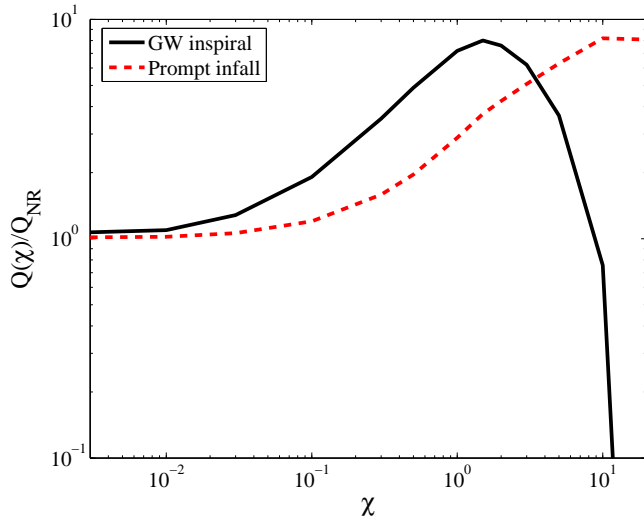


FIG. 5.— The x -dependence of the enhancement of the prompt infall and GW inspiral event rates by RR over NR, as expressed by the stellar current at the critical energy x_c , $Q(x_c; \eta) = Q(x_c; 0)$, for $x_c = x_p; x_{GW}$.

5. OBSERVABLE IMPLICATIONS OF RESONANT RELAXATION

Most previous estimates of the loss rates did not take into account RR. Here we show that RR can strongly influence the GW inspiral rate, and may play an important role in determining the dynamical structures observed in the inner GC.

5.1. Infall and inspiral processes

5.1.1. Prompt infall

Figure (5) shows the change in the estimated rates of prompt infall and inspiral due to the inclusion of RR, as function of the RR efficiency parameter η . RR does not significantly increase the rate of prompt infall events. This result has already been demonstrated by the N -body simulations of RT96 and RI98, and is explained by the fact that most tidally disrupted stars originate from low- E orbits with $E \ll E_h$ (Lightman & Shapiro 1977; Baumgardt et al. 2005), where

mass precession suppresses scalar RR. Our analysis is complementary to that of RT96 and RI98 in that they took into account relaxation in J -space, but not in E -space, whereas ours explicitly solves self-consistently the DF and star current in E -space, but does not deal with the flow in J -space. Our results confirm the conclusion that for the likely value of the RR efficiency factor $\eta = 1$, the tidal disruption rate is enhanced by RR by only a factor of ~ 3 (Figs 3, 5). We note, however, that for higher values of η , the tidal disruption rate may increase significantly.

5.1.2. Gravitational wave inspiral

The detection of GW emission from compact remnants inspiraling into MBHs (EMRIs), is one of the major goals of the planned space-borne *LISA* GW detector⁶. The predicted event rate per galaxy is very uncertain, as estimates vary in the range $\text{Gyr}^{-1} \cdot \text{G}_W \cdot \text{Myr}^{-1}$ per galaxy (e.g. Hills & Bender 1995; Sigurdsson & Rees 1997; Ivanov 2002; Freitag 2001, 2003; Hopman & Alexander 2005).

Only stars originating from tightly bound orbits with energies E & E_{GW} can complete their inspiral and reach a high-frequency orbit observable by *LISA*, without being scattered prematurely into the MBH or to a wider orbit. An approximate upper-limit for the semi-major axis from which inspiral is possible can be obtained by equating the inspiral time t_{GW} with $(1 - \eta)T_{NR}$, the NR timescale for scattering by $J \sim J_c$, (Hopman & Alexander 2005),

$$a_{GW} = \frac{8^p}{c^2} \frac{GM}{E_1 T_h} \frac{E_1 T_h}{c^2} \approx \frac{85}{3} \frac{M}{2^3} \frac{c^2}{M}; \quad (35)$$

(the corresponding critical energy is $E_{GW} = GM/2a_{GW}$). There are three phases in the orbital evolution of a star that ends up as a GW source. The first is a scattering-dominated phase in J -space, where energy losses are negligible. This is followed by a transition phase, when $J \sim J_{SO}$, GW dissipation becomes significant, and the inspiral time is comparable to the scattering time. Finally, the star spirals in by GW emission so rapidly that it effectively decouples from the gravitational perturbations of the background stars. The value of a_{GW} is determined in the second, transition phase by the interplay between angular momentum relaxation and GW dissipation. The J -values typical of the transition phase are also those where GR-precession quenches RR, at $J < J_{Q_{RR}} \sim J_{SO}$ (Eq. 6). As a result, a_{GW} is still determined by NR through Eq. (35) even when RR dominates the dynamics at $J \sim J_{L_{SO}}$.

To verify that RR does not significantly affect the transition phase of inspiral and the value of the critical energy, we followed the approach used by Hills & Bender (1995) and Hopman & Alexander (2005), who performed Monte Carlo (MC) simulations of the scattering of stars in J -space. We compare the case where $T_J^s = T_{NR}$ (as was assumed in Hills & Bender 1995; Hopman & Alexander 2005) to the case where T_J^s includes RR (Eq. 11). Figure (6) shows our results in terms of the inspiral fraction $S(a)$, the fraction of MC experiments that end with the star spiraling in, relative to the total, which also includes the experiments that end with the star plunging directly into the MBH without emitting a detectable GW signal (the third possibility of diffusion to lower energies is

⁶ <http://lisa.jpl.nasa.gov/>

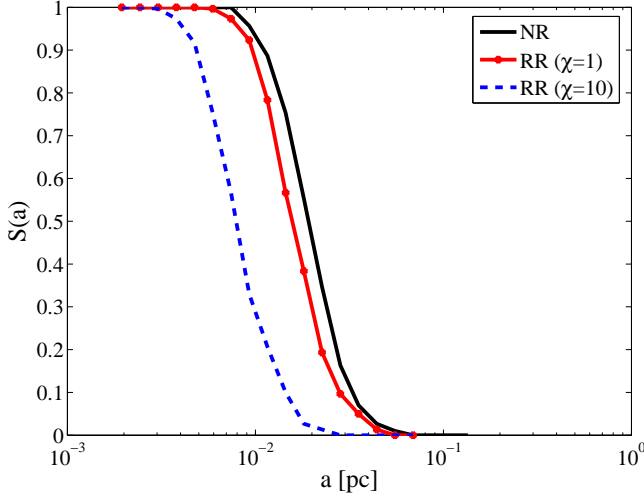


FIG. 6.— The fraction of stars $S(a)$ that produce a detectable GW signal out of all stars consumed by the MBH, as function of the initial semi-major axis. The solid line is for NR only; the dots for NR and RR (including GR quenching near $J_{\perp c}$). The two plots are almost identical, proving that RR does not affect the inspiral probability. The dashed line is for NR and RR, but with an artificially decreased GR precession (by a factor 10). In this case $S(a)$ drops at slightly smaller values of a . The small difference implies that $S(a)$ is not sensitive to the exact value of J_Q where RR is quenched.

not relevant here since only J -scattering is considered). The critical semi-major axis corresponds to $S(a_{GW}) = 0.5$. Figure (6) shows that RR has little effect on the value of a_{GW} , which is completely determined by NR. Furthermore, the outcome is not sensitive to the exact value of J_Q where RR is quenched, as is demonstrated by the fact that a_{GW} is only slightly decreased when the strength of GR precession is artificially lowered by a factor of 10 (by increasing J_Q to 10), which is equivalent to assuming a smaller value of J_Q .

Because $S(a)$ is well approximated by a step function at a_{GW} (or equivalently, $S(E)$ is a step function at E_{GW}), the inspiral event rate per galaxy *without* RR can be estimated by (Hopman & Alexander 2005)

$$\frac{GW}{NR} = f_s \int_{E_{GW}}^{\infty} \frac{dE n(E)}{\ln(J_c = J_{LSO}) T_{NR}(E)}; \quad (36)$$

where f_s is the population fraction of the specific GW sources under consideration (e.g. white dwarfs).

Figure (5) shows that the GW inspiral event rate reaches its maximal enhancement, of about an order of magnitude, for $\chi = 1$ and is enhanced over a wide range of values. Only when $\chi = 10$ is the RR depletion of high energy GW inspiral candidates with $\chi \approx \chi_{GW}$ so strong (Fig. 2) that the GW inspiral rate falls below that predicted for NR only. This depletion can be expressed by introducing an effective high-energy cutoff $E_{RR} = E_D$, such that $n(E) = 0$ for $E > E_{RR}$. Two very different situations can occur, depending on whether the critical energy E_{GW} is larger or smaller than the cutoff energy E_{RR} .

If $E_{GW} > E_{RR}$, the DF vanishes for all energies where stars could complete their inspiral. In this case the GW event rate is vanishingly small. Fortunately for the prospects of EMRI detection, it appears likely that this is *not* the case (see Figs. 3, 4, 5). When $E_{GW} < E_{RR}$, the GW event rate is given by

$$\frac{GW}{tot} = \frac{GW}{NR} + f_s \int_{E_{GW}}^{\infty} \frac{dE n(E)}{T_{RR}^s(E)} = f_s I_0 Q(\chi_{GW}); \quad (37)$$

where the last equality follows from Eq. (27) in steady state.

The Galactic MBH is the prototypical *LISA* target (the orbital frequencies around more massive MBHs are below the *LISA* sensitivity band). Applying our result to the GC, we estimate that RR increases the predicted *LISA* event rate per galaxy by up to a factor (Fig. 3)

$$\frac{GW}{tot} = \frac{Q_{RR}(\chi_{GW})}{Q_{NR}(\chi_{GW})} \approx 8; \quad (38)$$

over previous predictions that assumed NR only. One caveat is that our analysis neglects the effects of mass segregation in a multi-mass population. For example, low-mass remnants will be driven by mass segregation to a flatter density distribution, which will decrease their contribution to the inspiral event rate (Hopman & Alexander 2005, 2006), and the opposite will happen for high mass objects. Here we do not consider a multi-mass population.

5.2. Resonant relaxation in the Galactic center

At a distance of ≈ 8 kpc (Reid & Bruthaler 2004), the Galactic MBH is the closest and most accessible MBH. Astrometric and radial velocity measurements of stars closely orbiting the MBH indicate that its mass is $M \approx 3.4 \times 10^6 M_\odot$ (Schödel et al. 2002; Ghez et al. 2003; Eisenhauer et al. 2005; for a review see Alexander 2005). Observations of the GC provide the most detailed information available about stars close to a MBH, where the orbits are Keplerian. The Galactic MBH offers, in principle, the best chances of confronting RR with observations. We consider here the implications of RR for several observed and predicted features of the GC: the young coherent star disks, the central randomized cluster and the relaxed old giants; the orbital parameters of the innermost stars; the stellar density distribution; and the hypothesized dense stellar cluster of stellar black holes (SBHs).

Figure (7) compares the distance scales and the ages or lifespans of the various dynamical structures and components in the inner pc of the GC with the relaxation timescales. The NR timescale in the GC, which is roughly independent of radius, is $T_{NR} \approx 10^8$ yr (Eq. 1). The scalar RR relaxation time T_{RR}^s is shown for $\chi = 1; 10$, or, equivalently, for $M_\bullet = 1; 10 M_\odot$ with $\chi = 1$. At large radii the RR time decreases towards the center, but for small radii, where GR precession becomes significant, it increases again (see §2). The vector RR timescale T_{RR}^v , in contrast, decreases unquenched with decreasing radius. Structures whose estimated age exceeds these relaxation timescales must be relaxed. Structures whose lifespan exceeds the relaxation timescales may be affected, unless we are observing them at an atypical time soon after they were created. As is further discussed below, RR can naturally explain some of the systematic differences between the various dynamical components in the GC.

The observed deviations from spherical symmetry of the potential in the GC do not affect RR. As an example, one may consider a ring of mass M_r and radius r . Such a perturbation to the potential would change orbits with semi-major axis a on the Kozai time (Kozai 1962) $t_K \approx 2 \pi (M_\bullet / M_r) (r/a)^3 P(a)$, which is larger than t_M by a factor of order $t_K / t_M \approx 2 \pi N (< a) M_\bullet / M_r (r/a)^3 \approx 2 \pi N (< r) M_\bullet / M_r$. This implies that

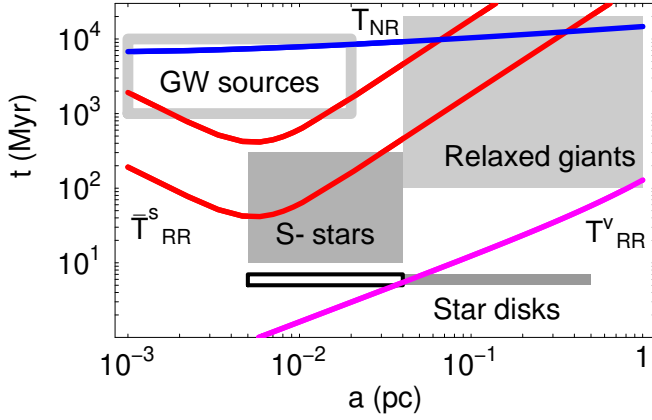


FIG. 7.— Stellar components, timescales and distance scales in the GC (equating $a = r$). The NR timescale T_{NR} (top straight line); the averaged scalar RR timescale T_{RR}^s , estimated for $1M_\odot$ stars (top curved line) and $10M_\odot$ stars (bottom curved line); the vector RR timescale T_{RR}^v (bottom straight line); the position and estimated age of the young stellar rings in the GC (filled rectangle in the bottom right); the position and age of the S-stars if they were born with the disks (empty rectangle in the bottom left); the position and maximal lifespan of the S-stars (filled rectangle in the middle left); the position and age of the dynamically relaxed old red giants (filled rectangle in the top right); and the position and age of the reservoir of GW inspiral sources, where the age is the progenitor's age or the time to sink to the center (empty rectangle in the top left).

only if the mass of the ring is comparable to the enclosed mass, such a perturbation to sphericity will be important. This is not the case in the GC. For example, the heaviest young stellar disk has a mass $M_r < 10^4 M_\odot$ (Nayakshin et al. 2006), giving $t_K = t_M > 400$ for $r = 0.4$ pc.

5.2.1. RR and the young stars in the Galactic center

Two distinct young stellar populations in the GC may be of particular relevance for testing RR. At distances of 0.04 – 0.5 pc from the MBH there are about 70 young massive OB stars ($M_\odot \gtrsim 10 M_\odot$, lifespan of $t_\odot = 6$ – 2 Myr), which are distributed in two nearly perpendicular, tangentially rotating disks (Levin & Belobodorov 2003; Genzel et al. 2003; Paumard et al. 2005). It appears that these stars were formed by the fragmentation of gas disks (Levin & Belobodorov 2003; Levin 2003; Nayakshin & Cuadra 2004; Nayakshin & Sunyaev 2005; Nayakshin 2006). This young population coexists with a relaxed population of long-lived evolved giants ($t_\odot > 100$ Myr, $M_\odot \gtrsim 8 M_\odot$; Genzel, Hollenbach & Townes 1994). Inside the inner 0.04 pc the population changes. There is no evidence for old stars, and the young stars there (the “S-stars”) are main-sequence B-stars ($M_\odot \gtrsim 15 M_\odot$, lifespans of 10^7 , $t_\odot \gtrsim 2$ – 10^8 yr; Ghez et al. 2003; Eisenhauer et al. 2005) on randomly oriented orbits with a random (thermal) \mathcal{J} -distribution. The orbital solutions obtained for a few of the S-stars indicate that they are tightly bound to the MBH (Ghez et al. 2003; Eisenhauer et al. 2005). There is to date no satisfactory explanation for the presence of the S-stars so close to the MBH (see Alexander 2005 for a review). One possibility is that they originated far from the MBH and were captured near it by dynamical exchange interactions (Gould & Quillen 2003; Alexander & Livio 2004). In that case only their lifespan can be confidently determined, but not their actual age. Another possibility is that they also originated in the star disks. In that case their age is the same as that of the disks and is much shorter than their lifespan.

The existence of coherent dynamical structures in the GC

constrains the relaxation processes on these distance scales, since the relaxation timescales must be longer than the structure age t_\odot to avoid randomizing it. Figure (7) shows that the observed systematic trends in the spatial distribution, age and state of relaxation of the different stellar components of the GC are consistent, and perhaps even caused by RR. The star disks are young enough to retain their structure up to their inner edge at 0.04 pc where $t_\odot \approx T_{RR}^v$ and vector RR can randomize the disk. It is tempting to explain the S-stars as originally being the inner part of the disk. However, RR alone cannot explain why the S-stars are systematically less massive than the disk stars. Regardless of their origin, their random orbits are consistent with the effect of RR. Vector RR can also explain why the evolved red giants beyond 0.04 pc, in particular the more massive ones with $t_\odot \approx \ln(T_{NR}/T_{RR}^s)$ are relaxed, since $T_{RR}^v < t_\odot$ out to ~ 1 pc. Note that scalar RR is in itself not efficient enough to drain the S-stars, but it can play a role in their non-zero eccentricities (see also Levin 2006).

Rapid RR changes the orbital eccentricities. On the timescales relevant for observations ($t \sim t_\odot$; Eq. 4), the change grows linearly and could be detected, in principle, by precision astrometry. However, the effect is small. In the linear regime the shortest time-scale for changes in \mathcal{J} is determined by scalar RR. The fractional change per orbit is $\mathcal{J}_P = \mathcal{J}_C \frac{N(<a)(M_\odot \approx M_\odot)}{N(<a)(M_\odot \approx M_\odot) - 1} \approx \frac{e}{e_0}$ (Eq. 2), which corresponds to a change in eccentricity of $e_P \approx \frac{e}{e_0} - e$. For the best measured orbit (the star S2 with $e = 0.8760 \pm 0.0072$, Eisenhauer et al. 2005) the predicted change per orbit is $e_P \approx 10^{-4}$ (assuming $M_\odot = 10 M_\odot$, $a = 0.01$ pc and $N(<a) = 2500$). This is beyond the current astrometric precision.

5.2.2. RR and the stellar distribution in the Galactic center

Figure (8) shows the density distribution $n(r)$ (Eqs. 20, 22) and the distribution of semi-major axis $a^2 n(a)$ (Eq. 21) for a model of the GC with different values of β . The central depletion in the distribution of the semi-major axis (or equivalently, energy) does not appear in the space density profile, because unbound and weakly bound stars on eccentric orbits spend a fraction of their orbit in the center. The effect of RR on the density distribution only appears as a gradual flattening of the cusp slope to $n_u(r) \propto r^{-1/2}$ (Eq. 22). The effect on the observed projected surface density distribution will be even less noticeable. RR is predicted to flatten the density distribution only at $r \lesssim 10^3$ pc, for $\beta = 1$. Farther out the distribution is virtually identical with the NR solution. Since there are no observational data on the density distribution for distances $> 5 \times 10^3$ pc (Schödel et al. 2005), it is presently not possible to test this aspect of RR in the GC. However, if $\beta = 1$, the space density will flatten farther out, on a length-scale that may be observationally accessible. It should be emphasized that any detailed comparisons between the observed stellar distribution and models will likely be difficult (Alexander 1999, 2005). The observed density profile in the inner 0.4 pc falls as $n(r) \propto r^{-1.4}$ (Genzel et al. 2003), less steeply than predicted by the single mass BW76 solution. It is highly likely that additional dynamical processes beyond the simple picture considered here are at work, such as mass segregation (BW77). Furthermore, a large fraction of this observed distribution is comprised of massive stars with lifespans shorter than either the NR or RR relaxation times (Fig. 7); these stars probably do not trace the relaxed population.

We note that if the power-law profile were to continue to

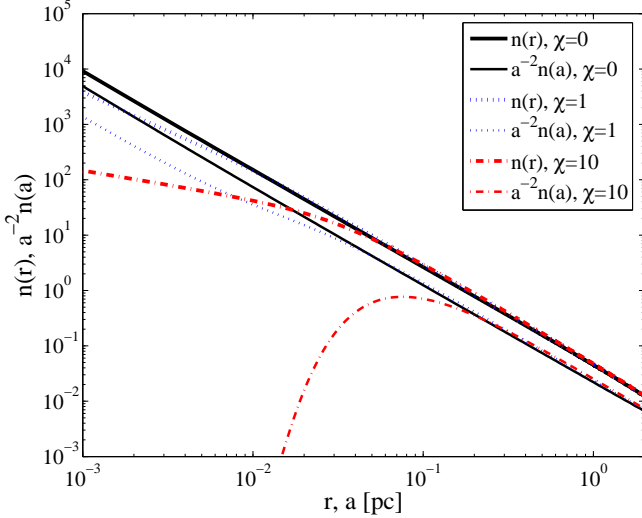


FIG. 8.— The density profile $n(r)$ and the distribution of the semi-major axis $n(a)$ in the GC for several values of χ .

very small radii, the smallest radius r_1 where a star is still statistically expected to be found, $r_1 = N_h^{1/(3-\gamma)} r_h \approx 6 \times 10^5 \text{ pc}$ (for $\gamma = 1.4$), would be well inside radius where RR depletes the cusp. If such a yet undetected population of tightly bound stars exists, it should exhibit an exponential central suppression at $\approx 10^3 \text{ pc}$.

5.2.3. RR and dark mass in the Galactic Center

It is likely that the Galactic MBH is surrounded by a dynamically significant distribution of dark mass in the form of compact remnants, in particular SBHs that have sunk to the center by mass-segregation over the lifetime of the Galaxy (Morris 1993; Miralda-Escudé & Gould 2000; Hopman & Alexander 2006; Freitag, Amaro-Seoane & Kalogera 2006). The existence of dark matter can be constrained by detecting orbital deviations from purely Keplerian motions (Mouawad et al. 2004; Alexander 2005). The co-existence of a dense cluster of SBHs with the dense stellar cusp may have interesting dynamical implications (e.g. Alexander & Livio 2004). Efficient RR could deplete this dark mass component by rapidly draining the compact remnants into the MBH. For our assumed RR efficiency factor $\chi = 1$ the depletion will be significant only on scales $< \text{few} \times 10^3 \text{ pc}$ (Fig. 8) with negligible dynamical implications for the observed stars. However, if $\chi \approx 10$, the inner 0.01 pc will be depleted. Future high resolution observations of stellar orbits may therefore further constrain RR.

RR may also affect the emission of gamma rays by annihilation of hypothetical dark matter (DM) particles near MBHs. It was shown that gravitational scattering between DM and stars leads to a DM density profile $\rho_{\text{DM}} \propto r^{-3/2}$ (Gnedin & Primack 2004; Merritt 2004). This profile implies an annihilation rate which is proportional to $\log(r_{\text{h}}/r_{\text{in}})$. In presence of RR, the inner cut-off of the cusp r_{in} will be large as compared to the situation discussed in the literature where RR is absent, thus somewhat decreasing the annihilation rate.

6. DISCUSSION AND SUMMARY

RR is a coherent relaxation process that operates when symmetries in the gravitational potential restrict the evolution of

the orbits (R96; RI98; Tremaine 2005). As a result, the orbits maintain their orientation over many orbital periods, and over that time the stars exert coherent mutual torques. These efficiently change the orbital angular momentum J (energy relaxation continues on the slow NR timescale). RR operates only under specific conditions. However, when these are met, it can be orders of magnitude more efficient than NR. Here we consider *scalar* RR, which affects both the direction and magnitude of J , in the regime around a MBH where the orbits are Keplerian (where both mass and GR precession are negligible), and *vector* RR, which affects the direction but not the magnitude of J , in the regime around a MBH where the potential is spherical. Scalar RR can deflect stars into the MBH, whereas vector RR can only change their orbital orientation.

In this paper we studied the effect RR has on the energy DF of stars near a MBH. We explored the consequences for the disruption and capture of stars by the MBH, in particular through inspiral by GW emission, and used our results to interpret the properties of the observed dynamical components in the GC. The complex full 2+1 $(E; J; t)$ problem was reduced to an approximate 1+1 $(E; t)$ Fokker-Planck equation, which we solved numerically. We also carried out Monte Carlo experiments to test some of our assumptions.

Our results are as follows. (1) RR leads to the depletion of the high-energy end of the DF (stars tightly bound to the MBH), accompanied by an enhanced current of stars to high energies. The exact extent of the depletion and the effective high-energy cutoff depend on the poorly determined efficiency of RR. The currently available estimates of the RR efficiency factor indicate that $\chi \approx 1$. (2) We confirm the result of RT96 that for $\chi = 1$, the direct tidal disruption rate is only modestly enhanced by RR. This is because scalar RR is most efficient close to the MBH where the orbits are Keplerian, whereas most of the tidally disrupted stars originate farther away from the MBH. A higher RR efficiency than assumed here could substantially *increase* the tidal disruption rate. (3) We show, in contrast, that the GW inspiral rate is dominated by RR dynamics, and is likely increased by almost an order of magnitude relative to the rate predicted assuming NR only. This is because stars undergoing GW inspiral originate very close to the MBH. A higher RR efficiency than assumed here could substantially *decrease* the GW inspiral rate by completely depleting the tightly bound stars. (4) We apply our results to the GC and show that vector RR can naturally explain the inner cutoff of the ordered star disks at 0.04 pc and the transition to the randomized inner S-star cluster, as well as the randomized state of the old red giants in the inner 1 pc . We also show that scalar RR is consistent with the presence of the disks, as it is too slow to disrupt them. If the S-stars were born in the disk on circular orbits, then scalar RR may explain their present non-zero eccentricities.

We note that there are additional processes that could be affected by RR, which we did not study here. Stars that undergo tidal capture and subsequent tidal heating (“squeeze-stars”, Alexander & Morris 2003) also originate close to the MBH, where RR dominates the dynamics. Squeeze-stars could be directly observed in the GC if RR substantially enhances their rates. A similar process is the tidal capture of a binary companion by an intermediate mass black hole in a young cluster and the subsequent Roche-lobe feeding that could power an ultra-luminous X-ray source (Hopman, Portegies Zwart & Alexander 2004; Hopman & Portegies Zwart 2005; Baumgardt et al. 2005). The role of RR in tidal capture is still unclear, as there is no RR quenching by GR precession at the

tidal capture radius that can stop the star from being rapidly destroyed.

There are several limitations and uncertainties in our results that will have to be addressed by future studies. Our treatment of the problem in E -space incorporates the RR sink terms in approximate form only. The efficiency of RR is poorly determined as it has been calibrated based on a restricted set of N -body simulations and its dependence on the parameters of the stellar system has not been investigated in full. This uncertainty is significant, as it could potentially reverse the sign of the effect of RR on the GW inspiral rate. While the rate is increased by an order of magnitude if $\beta = 1$, it is completely suppressed if $\beta \gg 10$ (Fig. 5). An important omission in our treatment is the assumption of a single mass stellar population. A multi-mass population will induce mass segregation. This will modify the DF directly (BW77), and likely also change the RR efficiency. The stellar DF also depends on processes that destroy one type of star while not affecting others, such as stellar collisions (e.g. Freitag & Benz 2001; 2002).

Progress on these issues will likely require large scale numerical simulations. The effects of RR on the DF of stellar systems with MBHs have not yet been studied by N -body simulations. The recent fully self-consistent N -body simulations of Baumgardt et al. (2004a, 2004b), Preto et al. (2004) and Merritt & Szell (2005), indicate that such studies are almost within reach of current hardware. Such simulations are particularly important for predicting GW inspiral rates, as these depend on a combination of complex mech-

anisms, including mass-segregation and RR, which are hard to assess with (semi-) analytical methods (e.g. Baumgardt et al. 2005). Our analysis shows that it may be of considerable importance to use a relativistic potential in such simulations (see e.g. Rauch 1999), since otherwise it is unclear whether RR is quenched, and a large number of stars may fall directly into the MBH without emitting an observable GW signal. Yet larger-scale modeling will require abandoning the exact N -body approach in favor of approximate methods such as Monte Carlo simulations with RR (Freitag & Benz 2001, 2002) or numerical 2+1 Fokker-Planck models.

We note that throughout we assumed a spherically symmetric DF. Deviations from spherical symmetry may affect both RR and the loss-cone structure in phase-space (see e.g. Magorrian & Tremaine [1999], who discuss the possibility of a loss 'wedge' in case of a triaxial DF). Typically this enhances the event rates.

Finally, we note that the observed dynamics of the GC provide a promising empirical basis for calibrating and cross-checking theoretical and numerical studies of RR.

We thank K. Rauch for comments on the numerical results of RT96 and A. Gualandris for her adaption of the N -body code by J. Makino and P. Hut (<http://www.artcompsci.org>). TA is supported by ISF grant 295/02-1, Minerva grant 8484, and a New Faculty grant by Sir H. Djangoly, CBE, of London, UK.

APPENDIX

A. THE LOGARITHMIC FORM OF THE FOKKER PLANCK EQUATION

Because of the large ratio of the tidal radius and the radius of influence, the natural way to integrate the Fokker-Planck equation is to divide the energy range into equal logarithmic intervals. For convenience we give here the equations in terms of the logarithmic distance variable $z = \ln(1 + x)$. The Fokker-Planck equation (27) without sink terms is then written as

$$\frac{\partial g(z;)}{\partial t} = (\epsilon - 1) \frac{\partial}{\partial z} \left(e^z \frac{\partial g(z;)}{\partial z} \right); \quad (A1)$$

where $Q = \sum_{i=1}^4 Q_i(z;)$ with

$$\begin{aligned} Q_1(z;) &= g(z;) \left(e^z - 1 \right)^{3/2}; \\ Q_2(z;) &= g(z) \int_z^{z_D} dw (e^w - 1)^{3/2} \frac{\partial g(w;)}{\partial w}; \\ Q_3(z;) &= e^z (e^z - 1)^{3/2} \frac{\partial g(z;)}{\partial z} \int_1^z dw e^w g(w); \\ Q_4(z;) &= e^z \frac{\partial g(z;)}{\partial z} \int_z^{z_D} dw (e^w - 1)^{3/2} e^w g(w); \end{aligned} \quad (A2)$$

The logarithmic expressions for the sink terms can be included directly from Eq. (27) by replacing $x \rightarrow e^z - 1$. Written this way, the numerical integration is simple and can be easily done over many orders of magnitude in energy.

B. THE NON-RESONANT LOSS-CONE SINK TERM

For convenience we reproduce here Eq. (14) of BW77, which interpolates between the empty and the full loss-cone regimes of the NR sink term,

$$R_{NR}(x;) = \frac{0.5 g(x;) x^{5/2}}{\ln(M - M_?) [5.56 + \ln(x_D = 4x) - q(x;)]}; \quad (B1)$$

where

$$M_? = M)^2 n_h r_h^3 x_D; \quad q(x;) = 1.6 \ln(6M - M_?) x^{5/2} g(x;); \quad (B2)$$

REFERENCES

- Alexander, T., 1999, *ApJ*, 520, 137
 Alexander, T., & Hopman, C., 2003, *ApJ*, 590, L29
 Alexander, T., & Morris, M., 2003, *ApJ*, 590, L25
 Alexander, T., & Livio, M., 2005, *ApJ*, 606, L21
 Alexander, T., 2005, *Physics Reports*, 419(2–3), 65
 Bahcall, J. N., & Wolf, R. A., 1976, *ApJ*, 209, 214 (BW76)
 Bahcall, J. N., & Wolf, R. A., 1977, *ApJ*, 216, 883 (BW77)
 Barack, L., & Cutler, C., 2004, *PRD*, D70, 122002
 Baumgardt, H., Makino, J., & Ebisuzaki, T., 2004a, *ApJ*, 613, 1133
 Baumgardt, H., Makino, J., & Ebisuzaki, T., 2004b, *ApJ*, 613, 1143
 Baumgardt, H., Hopman, C., Portegies Zwart, S. F., & Makino, J., 2005 (astro-ph/0511752)
 Binney, J. & Tremaine, S., 1987, *Galactic Dynamics* (Princeton: Princeton Univ. Press)
 Chandrasekhar, S., 1943, *Reviews of Modern Physics*, 15, 1
 Cohn, H., & Kulsrud, R. M. 1978, *ApJ*, 226, 1087
 Eisenhauer, et al., 2005, *ApJ*, 628, 246
 Ferrarese, L., & Merritt, D., 2000, *ApJ*, 539, L9
 Frank, J., Rees, M. J., 1976, *MNRAS*, 176, 633
 Freitag, M., & Benz, W., 2001, *A&A*, 375, 711
 Freitag, M. & Benz, W., 2002, *A&A*, 394, 345
 Freitag, M., 2001, *Class. Quantum Grav.*, 18, 4033
 Freitag, M., 2003, *ApJ*, 583, L21
 Freitag, M. & Benz, W., 2005, *MNRAS*, 358, 1133
 Freitag, M., Amaro-Seoane, P., & Kalogera, V., pre-print: astro-ph/0603280
 Gair, J. R., Barack, L., Creighton, T., Cutler, C., Larson, S., L., Phinney, E. S., Vallisneri, M., 2004, *Class. Quant. Grav.* 21, S1595
 Gebhardt, K., et al., 2000, *ApJ*, 539, L13
 Genzel, R. et al., 2003, *ApJ*, 594, 812
 Genzel, R., Hollenbach, D. & Townes, C. H., 1994, *Rep. Prog. Phys.*, 57, 417
 Ghez, A. M., et al., 2003, *ApJ*, 586, L127
 Gnedin, O. Y., & Primack, J. R., 2004, *PRL*, 93, 1302
 Gould, A., & Quillen, A., 2003, *ApJ*, 592, 935
 Hils, D., & Bender, P. L., 1995, *ApJ*, 445, L7
 Hopman, C., Portegies Zwart, S.F., & Alexander, T., 2004, *ApJ*, 604, L101
 Hopman, C., & Alexander, T., 2005, *ApJ*, 629, 362
 Hopman, C., & Alexander, T., 2006, pre-print: astro-ph/0603324
 Hopman, C., & Portegies Zwart, S. F., 2005, *MNRAS*, 363, L56
 Ivanov, P. B., 2002, *MNRAS*, 336, 373, 2002
 Kozai, Y., 1962, *AJ*, 67, 591
 Levin, Y., & Belobodorov, A. M., 2003, *ApJ*, 596, 314
 Levin, Y., 2003, (astro-ph/0307084)
 Levin, Y., 2006, *MNRAS*, submitted
 Lightman, A. P., Shapiro, S. L., 1977, *ApJ*, 211, 244
 Magorrian, J., Tremaine, S., 1999, *MNRAS*, 309, 447
 Marchant, A.B., & Shapiro, S.L., 1979, *ApJ*, 234, 317
 Marchant, A.B., & Shapiro, S.L., 1980, *ApJ*, 239, 685
 Merritt, D., 2004, *PRL*, 92, 1304
 Merritt, D., & Poon, M. Y., 2004, *ApJ*, 606, 788
 Merritt, D., & Szell, A., 2005 (astro-ph/0510498)
 Miller, M. C., Freitag, M., Hamilton, D. P., & Lauburg, V. M., 2005, *ApJ*, 631, L117
 Miralda-Escudé, J., & Gould, A., 2000, *ApJ*, 545, 847
 Morris, M., 1993, *ApJ*, 408, 496
 Mouawad, N., Eckart, A., Pfalzner, S., Schödel, R., Moulata, J., Spurzem, R., 2004, *Astronomische Nachrichten*, Vol. 326, 2, 83-95
 Murphy, B. W., Cohn, H. N., & Durisen, R. H., 1991, *ApJ*, 370, 60
 Nayakshin, S., & Cuadra, J., 2004, *A&A*, 437, 437
 Nayakshin, S., Sunyaev, 2005 (astro-ph/0507687)
 Nayakshin, S., Dehnen, W., Cuadra, J., & Genzel, R., 2006, *MNRAS*, 366, 1410
 Nayakshin, S., 2006 (astro-ph/0512255)
 Paumard, T., et al., 2005, *ApJ*, submitted
 Peters, P. C. 1964, *Phys. Rev.*, 136, 1224
 Preto, M., Merritt, D., Spurzem, R., 2004, *ApJ*, 613, L109
 Rauch, K. P., & Tremaine, S., 1996, *New Astronomy*, 149 (RT96)
 Rauch, K. P., 1999, *ApJ*, 514, 725
 Rauch, K. P., & Ingalls, 1998, *MNRAS*, 299, 1231 (RI98)
 Reid, M. J., & Brunthaler, A., *ApJ*, 616, 872
 Schödel, R. et al., 2002, *Nature*, 419, 694
 Schödel, R. et al., 2005, in prep.
 Shapiro, S.L., & Marchant, A.B., 1979, *ApJ*, 225, 603
 Sigurdsson, S., and Rees, M. J., 1997, *MNRAS*, 284, 318
 Syer, D., Ulmer, A., 1999, *MNRAS*, 306, 35
 Tremaine, S., et al., 2002, *ApJ*, 574, 740
 Tremaine, S., *ApJ*, 625, 143
 Wang, J., Merritt, D., 2004, *ApJ*, 600, 149